

Critical behavior in the antiperovskite ferromagnet AICMn₃Lei Zhang,^{1,*} Bosen Wang,^{2,†} Yuping Sun,^{1,2,‡} Peng Tong,² Jiyu Fan,³ Changjin Zhang,¹ Li Pi,^{1,4} and Yuheng Zhang^{1,4}¹High Magnetic Field Laboratory, Chinese Academy of Sciences, Hefei 230031, China²Key Laboratory of Materials Physics, Institute of Solid State Physics, Hefei 230031, China³Department of Applied Physics, Nanjing University of Aeronautics and Astronautics, Nanjing 210016, China⁴High Magnetic Field Laboratory, University of Science and Technology of China, Hefei 230026, China

(Received 15 December 2011; revised manuscript received 23 February 2012; published 29 March 2012)

We have investigated the critical behavior of the antiperovskite ferromagnetic AICMn₃ by bulk magnetization study. The critical exponents (β , γ , and δ) have been obtained by different methods, such as a modified Arrott plot, the Kouvel-Fisher method, and critical isotherm analysis. With these critical exponents, the experimental M - T - H relations below and above Curie temperature collapse into two universal branches, fulfilling the single scaling equation $m = f_{\pm}(h)$, where m and h are renormalized magnetization and field, respectively. The critical exponents are confirmed by the Widom scaling law $\delta = 1 + \gamma\beta^{-1}$. Apart from a slight increase in β and γ , the deduced critical exponents are very close to the theoretical values of the mean-field model, indicating the existence of a long-range ferromagnetic interaction. In addition, the exchange distance is obtained as $J(r) \sim r^{-4.7}$. We suggest that the competition between the localized Mn-Mn magnetic interaction and itinerant Mn-C hybridization should be responsible for the critical behavior in this system.

DOI: [10.1103/PhysRevB.85.104419](https://doi.org/10.1103/PhysRevB.85.104419)

PACS number(s): 75.40.Cx, 75.40.Gb

I. INTRODUCTION

The antiperovskite materials have attracted renewed attention due to their novel physical properties, such as superconductivity in MgCNi₃,¹ large magnetoresistance and magnetocaloric effect in GaCMn₃,^{2,3} nearly zero temperature coefficient of resistance and large magnetostriction up to 2000 ppm in CuNMn₃,^{4,5} and cracks induced by the magnetic ordering in ZnNMn₃.⁶ An antiperovskite with structural configuration AXM_3 (A represents main group element; X stands for carbon, boron, or nitrogen; and M is the transition metal) has a cubic structure of the perovskite type. In antiperovskite structure materials, X ions are located at the body-centered positions of the XM_6 octahedrons, M ions are located at the face-center positions, and A ions are located at the corner sites.⁷ Despite the isostructure of the perovskite, the physical properties of the transition-metal ions in the antiperovskite are very different from those in the perovskite owing to their different ionic occupations.

In Mn-based antiperovskite materials, AICMn₃ is prominent because of its large magnetocaloric effect near room temperature, which makes it a potential application for magnetic refrigeration with the advantage of being environmentally friendly.⁸ AICMn₃ exhibits a paramagnetic (PM)-ferromagnetic (FM) phase transition at the Curie temperature $T_C = 288$ K without magnetic hysteresis, and its resistivity shows a metallic behavior. Therefore, some previous investigations have proved that it is a soft itinerant ferromagnet.⁹⁻¹¹ Although the magnetothermal properties of AICMn₃ have been extensively investigated, more studies are desired to understand the intrinsic magnetic interactions. As shown in recent investigations, analysis of the critical exponents near the PM-FM region is an effective way to clarify the magnetic interactions and properties.¹²⁻¹⁴ In this paper, we study the critical behavior of AICMn₃, where the critical exponents β , γ , and δ have been obtained reliably by different analytical methods. It is found that the magnetic behavior of AICMn₃ is close to the theoretical prediction of the mean-field model,

except that β and γ are slightly larger than theoretical values. In addition, the magnetic interaction distance was deduced to decay as $J(r) \sim r^{-4.7}$.

II. EXPERIMENT

A polycrystalline sample of AICMn₃ was prepared by the solid-state reaction method. The detailed preparation procedure was described elsewhere.⁸ The magnetization was measured using a superconducting quantum interference device magnetometer (Quantum Design MPMS). The sample was processed to ellipsoid shape, and the magnetic field was applied along the longest semiaxis to decrease the demagnetizing field. In order to make sure each curve was initially magnetized, the isothermal magnetization was performed after the sample was heated well above T_C for a long enough time, then cooled under zero field to the objective temperature. The applied magnetic field H_a has been corrected into the internal field as $H_i = H_a - NM$ (where M is the measured magnetization and N is the demagnetization factor obtained as in Ref. 15). The calculated H_i was used for analysis of the critical behavior.

III. RESULTS AND DISCUSSION

Figure 1 displays the temperature dependence of magnetization $M(T)$ and inverse magnetization $M^{-1}(T)$ for AICMn₃. A PM-FM phase transition occurs at $T_C \sim 288$ K, which is determined from dM/dT (shown in the inset of Fig. 1), in agreement with previous reports.^{11,16} The $M(T)$ curve branches between the zero-field-cooling (ZFC) and field-cooling (FC) conditions, which may be due to magnetic disorders caused by atomic disorders. The deviation of $M^{-1}(T)$ from the straight line above T_C indicates the appearance of critical fluctuations even in the PM phase.¹⁷ Generally, H/M vs M^2 present a series of straight lines around T_C in ferromagnetic materials according to the Arrott plot, where H/M vs M^2 at T_C just pass through the origin.¹⁸ The slope of the line indicates the order

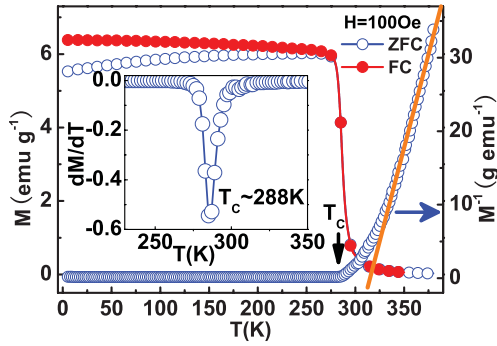


FIG. 1. (Color online) Temperature dependence of magnetization $M(T)$ (left axis) and inverse magnetization $M^{-1}(T)$ (right axis). The inset shows dM/dT vs T .

of the phase transition according to the criterion suggested by Banerjee: a negative slope corresponds to a first-order transition while positive slope corresponds to a second-order one.¹⁹ Figure 2(a) presents the initial isothermal magnetization around T_C at the interval of 2 K, and H/M vs M^2 around T_C are plotted in Fig. 2(b). It can be seen that all H/M vs M^2 relations show quasistraight lines with positive slopes in high field range, implying a second-order transition. However, these lines are not parallel to each other, indicating that $\beta = 0.5$ and $\gamma = 1.0$ within the framework of Landau mean-field model need to be modified.

It is well known that the critical behaviors for a second-order phase transition can be studied in detail through a series of critical exponents. In the vicinity of a second-order phase transition, the divergence of correlation length $\xi = \xi_0|$

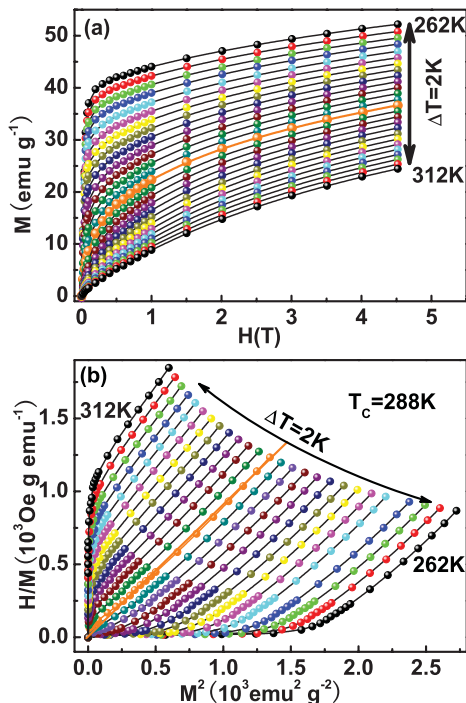


FIG. 2. (Color online) (a) The initial isothermal magnetization around T_C ; (b) Arrott plot of H/M vs M^2 .

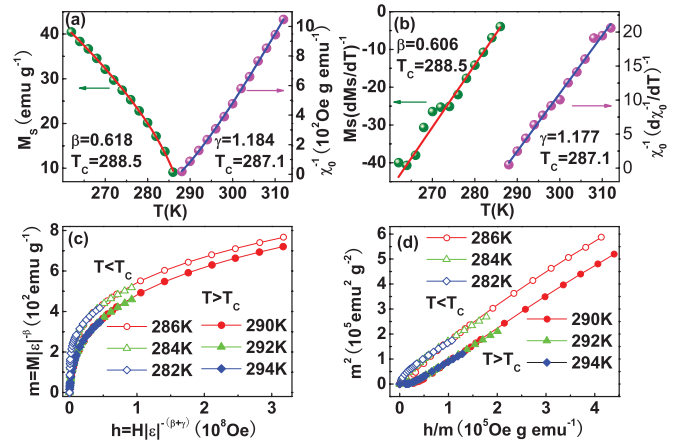


FIG. 3. (Color online) (a) The spontaneous magnetization M_S (left) and inverse initial susceptibility χ_0^{-1} (right) vs T with the fitting solid curves; (b) KF plots for $M_S(T)$ (left) and $\chi_0^{-1}(T)$ (right) (solid lines are fitted); (c) scaling plots around T_C using β and γ determined by the KF method (only a few typical curves are shown); (d) the renormalized magnetization and field potted as m^2 vs h/m .

$(T_C - T)/T_C|^{-\nu}$ leads to universal scaling laws for the spontaneous magnetization M_S and initial susceptibility χ_0 . In this sense, the mathematic definitions of exponents from magnetization can be described as^{20,21}

$$M_S(T) = M_0(-\varepsilon)^\beta, \quad \varepsilon < 0, \quad T < T_C, \quad (1)$$

$$\chi_0(T)^{-1} = (h_0/M_0)\varepsilon^\gamma, \quad \varepsilon > 0, \quad T > T_C, \quad (2)$$

$$M = DH^{1/\delta}, \quad \varepsilon = 0, \quad T = T_C, \quad (3)$$

where $\varepsilon = (T - T_C)/T_C$ is the reduced temperature and M_0/h_0 and D are critical amplitudes. The parameters β (associated with M_S), γ (associated with χ_0), and δ (associated with T_C) are the critical exponents. As shown in Fig. 3(a), M_S and χ_0^{-1} are obtained by linear extrapolation from the high-field region to the intercepts. According to Eqs. (1) and (2), it is obtained from the modified Arrott plot that $\beta = 0.618 \pm 0.002$ with $T_C = 288.5 \pm 0.1$ and $\gamma = 1.184 \pm 0.003$ with $T_C = 287.1 \pm 0.3$. One can see that the value of T_C obtained from the modified Arrott plot agrees well with that obtained from the $M(T)$ curve.

On the other hand, the critical exponents can be accurately determined by the Kouvel-Fisher (KF) method:²²

$$\frac{M_S(T)}{dM_S(T)/dT} = \frac{T - T_C}{\beta}, \quad (4)$$

$$\frac{\chi_0^{-1}(T)}{d\chi_0^{-1}(T)/dT} = \frac{T - T_C}{\gamma}. \quad (5)$$

According to Eqs. (4) and (5), $M_S(T)/[dM_S(T)/dT]$ and $\chi_0^{-1}(T)/[d\chi_0^{-1}(T)/dT]$ vs T should yield straight lines with slopes $1/\beta$ and $1/\gamma$, respectively. $M_S(T)/[dM_S(T)/dT]$ and $\chi_0^{-1}(T)/[d\chi_0^{-1}(T)/dT]$ vs T are plotted in Fig. 3(b). The new exponents are obtained as $\beta = 0.606 \pm 0.009$ with $T_C = 288.5 \pm 0.5$ and $\gamma = 1.177 \pm 0.008$ with $T_C = 287.1 \pm 0.6$ by the KF method. These values are close to those deduced from the modified Arrott plot.

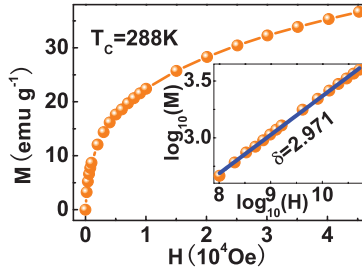


FIG. 4. (Color online) The critical isotherm analysis at T_c . The inset shows the plot on \log_{10} - \log_{10} scale with a fitted solid line.

According to the prediction of the scaling equation, in the asymptotic critical region, the magnetic equation can be written as²¹

$$M(H, \varepsilon) = \varepsilon^\beta f_\pm(H/\varepsilon^{\beta+\gamma}), \quad (6)$$

where f_\pm are regular functions with f_+ for $T > T_c$ and f_- for $T < T_c$. Equation (6) indicates that $M(H, \varepsilon)\varepsilon^{-\beta}$ vs $H\varepsilon^{-(\beta+\gamma)}$ forms two universal curves for $T > T_c$ and $T < T_c$, respectively. Defining the renormalized magnetization as $m \equiv \varepsilon^{-\beta}M(H, \varepsilon)$ and the renormalized field as $h \equiv H\varepsilon^{-(\beta+\gamma)}$, the scaling equation is rewritten as

$$m = f_\pm(h). \quad (7)$$

Based on the scaling equation, the isothermal magnetization around T_c is plotted in Fig. 3(c), where all experimental data collapse onto two universal curves. Alternatively, the exponents have been confirmed with a more rigorous method by plotting m^2 vs h/m as given in Fig. 3(d), which shows that all experimental data fall on two independent branches. The obedience of the scaling equation over the entire range of the normalized variables indicates the reliability of the obtained critical exponents.

The third critical exponent δ can be determined from the critical isotherm analysis according to Eq. (3). Obviously, from the above critical exponents, the Curie temperature can be determined to be 288 K. Figure 4 shows the isothermal magnetization at $T = 288$ K, where the inset shows the plot on the \log_{10} - \log_{10} scale. The $\log_{10}(M)$ - $\log_{10}(H)$ relation yields a straight line in the higher field range with the slope $1/\delta$. Subsequently, $\delta = 2.971 \pm 0.002$ is obtained. According to statistical theory, these critical exponents fulfill the Widom scaling relation:²³

$$\delta = 1 + \frac{\gamma}{\beta}. \quad (8)$$

As a result, $\delta = 2.92 \pm 0.02$ is obtained from the modified Arrott plot in Fig. 3(a), and $\delta = 2.94 \pm 0.06$ is deduced by the KF method in Fig. 3(b), which agree well with that obtained from the critical isotherm analysis.

According to the Arrott-Noakes equation of state, H/M vs M follows $(H/M)^{1/\gamma} = (T - T_c)/T_c + (M/M_1)^{1/\beta}$ (where M_1 is constant).²⁴ However, the Arrott-Noakes equation of state is only strictly obeyed at the limit of $\varepsilon \rightarrow 0$ ($T \rightarrow T_c$). More universally, H/M vs M obeys

$$(H/M)^{1/\gamma} = A' + B'M^{1/\beta}, \quad (9)$$

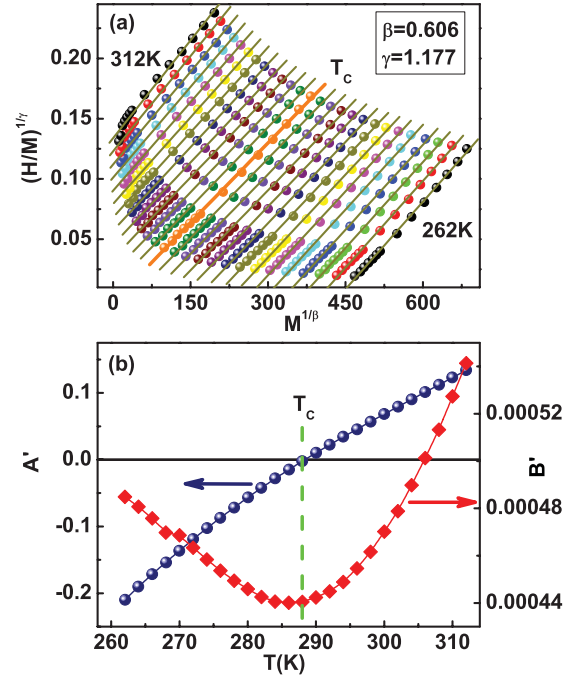


FIG. 5. (Color online) (a) The $(H/M)^{1/\gamma}$ vs $M^{1/\beta}$ with the critical exponents obtained by the KF method; (b) temperature dependence of modified coefficients A' and B' .

where A' and B' are temperature-dependent coefficients. Thus the experimental results are reconstructed as $(H/M)^{1/\gamma}$ vs $M^{1/\beta}$ with critical exponents obtained from the KF method, as depicted in Fig. 5(a). One can see that all lines are parallel to each other, where the line at T_c just passes through the origin. The obtained A' and B' are shown in Fig. 5(b). It is noticed that A' just passes the origin at T_c . In addition, the minimum of B' is located at T_c . All the results indicate that the obtained critical exponents are reliable.

The obtained critical exponents of AlCMn_3 , as well as those of different theoretical models, are listed in Table I for comparison. It is found that experimentally deduced β , γ , and δ are very close to values of the mean-field model, which indicates that the FM coupling in the sample is a long-range interaction. However, β and γ are slightly larger than the theoretical values. In view of the deviation of the estimated exponents from the theoretical values, it is important to clarify whether they belong to any universality class in the asymptotic region. Thus the effective exponents β_{eff} and γ_{eff} are obtained as²⁵

$$\beta_{\text{eff}}(\varepsilon) = \frac{d[\ln M_S(\varepsilon)]}{d(\ln \varepsilon)}, \quad \gamma_{\text{eff}}(\varepsilon) = \frac{d[\ln \chi_0^{-1}(\varepsilon)]}{d(\ln \varepsilon)}. \quad (10)$$

The β_{eff} and γ_{eff} as a function of reduced temperature ε are plotted in Figs. 6(a) and 6(b). However, both $\beta_{\text{eff}}(\varepsilon)$ and $\gamma_{\text{eff}}(\varepsilon)$ show nonmonotonic changes with ε , indicating that β_{eff} and γ_{eff} do not match any predicted universality class, even in the asymptotic region. This result resembles that in $\text{Pr}_{0.5}\text{Sr}_{0.5}\text{MnO}_3$ and partially frustrated amorphous alloys, where the nonmonotonic changes were attributed to magnetic disorders.^{15,25} As mentioned, the branching of the $M(T)$ curves under the ZFC and FC conditions also implies

TABLE I. Comparison of critical exponents of AlCMn_3 with different theoretical models. MAP, modified Arrott plot; KF, Kouvel-Fisher method; CI, critical isotherm analysis.

Composition	Reference	T_c (K)	β	γ	δ
AlCMn_3 (MAP)	This work	288.5 ± 0.1	0.618 ± 0.002	1.184 ± 0.003	2.92 ± 0.02^a
AlCMn_3 (KF)	This work	288.5 ± 0.5	0.606 ± 0.009	1.177 ± 0.008	2.94 ± 0.06^a
AlCMn_3 (CI)	This work	288			2.971 ± 0.002
Tricritical mean-field model	31		0.25	1.0	5.0
Mean-field model	32		0.5	1.0	3.0
3D Heisenberg model	32		0.365	1.386	4.8
3D Ising model	32		0.325	1.24	4.82

^aWidom scaling relation $\delta = 1 + \gamma\beta^{-1}$.

the existence of magnetic disorders, in agreement with the conclusion here. The magnetic disorders may be produced by atomic disorders in this system. As is known, there should be no magnetic disorders in an ideal AlCMn_3 sample. However, a few atomic disorders are unavoidable in the sample, which lead to magnetic disorders. Therefore, the branching of ZFC and FC may be attributed to the extrinsic magnetic disorders. However, for a second-order phase transition, the critical exponents for a homogeneous magnet should be independent of the microscopic details of the system due to the divergence of correlation length in the vicinity of the transition point.²⁶ Hence, the critical exponents obtained here are intrinsic.

For a homogeneous magnet, the universality class of the magnetic phase transition depends on the exchange interaction $J(r)$. A renormalization group theory analysis suggests the long-range attractive interactions decay as²⁷

$$J(r) \sim 1/r^{(d+\sigma)}, \quad (11)$$

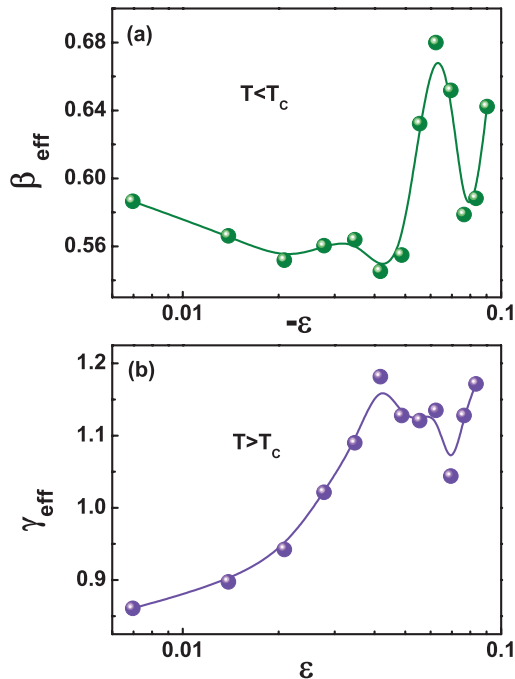


FIG. 6. (Color online) Effective exponents (a) β_{eff} and (b) γ_{eff} as a function of the reduced temperature ϵ .

where d is the spatial dimension and σ is a positive constant. For the long-range interaction, we have^{15,27,28}

$$\gamma = 1 + \frac{4n+2}{dn+8}\Delta\sigma + \frac{8(n+2)(n-4)}{d^2(n+8)^2} \times \left[1 + \frac{2G(\frac{d}{2})(7n+20)}{(n-4)(n+8)} \right] \Delta\sigma^2, \quad (12)$$

where $\Delta\sigma = (\sigma - \frac{d}{2})$, $G(\frac{d}{2}) = 3 - \frac{1}{4}(\frac{d}{2})^2$, and n is the spin dimensionality. For three-dimensional materials ($d = 3$), there is a relation $J(r) \sim r^{-(3+\sigma)}$ with $3/2 \leq \sigma \leq 2$. When $\sigma = 2$, the Heisenberg model ($\beta = 0.365$, $\gamma = 1.386$, and $\delta = 4.8$) is valid for the three-dimensional isotropic ferromagnet, where $J(r)$ decreases faster than r^{-5} . When $\sigma = 3/2$, the mean-field model ($\beta = 0.5$, $\gamma = 1.0$, and $\delta = 3.0$) is satisfied, which indicates that $J(r)$ decreases slower than $r^{-4.5}$. Herein, it is obtained that $\sigma = 1.734 \pm 0.003$ according to Eq. (12), implying that $J(r)$ decreases as $\sim r^{-4.7}$ in the ferromagnetic AlCMn_3 . It is noticed that $J(r)$ lies between that of the Heisenberg model and the mean-field model. In fact, in Mn-based antiperovskite, it has been suggested that there exist strong competitions between Mn-Mn and Mn-C bonds, where the Mn-Mn bonds are metallic and the Mn-C bonds are covalent.²⁹ Theoretical investigations have demonstrated that the density of states (DOS) at the Fermi level E_F [$N(E_F)$] is predominantly contributed by Mn $3d$ electrons in the Mn-based carbide antiperovskite.²⁹ However, there exist strong hybridization between Mn $3d$ states and C $2p$ states, which leads to the widening of the bandwidth of Mn $3d$ states as wide as 5 eV.^{29,30} Consequently, the electrons of the Mn $3d$ state are mainly itinerant in this system. In addition, the obtained saturated magnetic moment ($\mu_S = 1.15\mu_B \text{ Mn}^{-1}$) is much lower compared to that of the localized Mn ions in perovskite ($3 - 4 \mu_B \text{ Mn}^{-1}$), which also indicates an itinerant character of the carriers in AlCMn_3 .^{2,8} Therefore, the competition between the Mn-Mn and Mn-C bonds should be responsible for the exchange interaction $J(r)$ in this system. The Mn-Mn magnetic interaction tends to create a localized ferromagnetism. However, the Mn-C hybridization is inclined to form the itinerant state. Thus, the competition leads to an itinerant ferromagnetic state with $J(r)$ lying between the 3D Heisenberg model and the mean-field model.

IV. CONCLUSION

In summary, the critical behavior of AlCMn_3 has been investigated. Reliable critical exponents β and γ are obtained from the modified Arrott plot and KF method, and δ was generated by critical isotherm analysis. With these exponents, the M - T - H relations below and above T_C collapse into two universal branches in the asymptotic critical region following the scaling equation. Moreover, all critical exponents fulfill the Widom scaling law. It is found that the obtained critical exponents of AlCMn_3 approach close to the theoretical prediction of the mean-field model, except that β and γ are slightly larger. The investigation of critical behavior gives the result that the interaction distance decays as $J(r) \sim r^{-4.7}$, which lies between that of the Heisenberg model and mean-field model. We suggest that the competition between the localized Mn-Mn

magnetic interaction and itinerant Mn-C hybridization should be responsible for the critical behavior in this system.

ACKNOWLEDGMENTS

This work was supported by the National Key Basic Research under Contracts No. 2007CB925001, No. 2011CBA00111, and No. 2010CB923403; the National Natural Science Foundation of China under Contracts No. 50701042, No. 51001094, No. 11174295, No. 51171177, and No. 11004196; the Director's Fund of Hefei Institutes of Physical Science, Chinese Academy of Sciences, under Contract No. O84N3A1133; and the Knowledge Innovation Program of the Chinese Academy of Sciences through Grant No. 106CS31121 (Hefei Institutes of Physical Science, CAS).

*zhanglei@hmfl.ac.cn

†bswang@issp.ac.cn

‡ypsun@issp.ac.cn

¹T. He, Q. Huang, A. P. Ramirez, Y. Wang, K. A. Reran, N. Rogado, M. A. Hayward, M. K. Haas, J. S. Slusky, K. Inumara, H. W. Zandbergen, N. P. Ong, and R. J. Cava, *Nature (London)* **411**, 54 (2001).

²K. Kamishima, T. Goto, H. Nakagawa, N. Miura, M. Ohashi, N. Mori, T. Sasaki, and T. Kanomata, *Phys. Rev. B* **63**, 024426 (2000).

³T. Tohei, H. Wada, and T. Kanomata, *J. Appl. Phys.* **94**, 1800 (2003).

⁴E. O. Chi, W. S. Kim, and N. H. Hur, *Solid State Commun.* **120**, 307 (2001).

⁵K. Asano, K. Koyama, and K. Takenaka, *Appl. Phys. Lett.* **92**, 161909 (2008).

⁶W. S. Kim, E. O. Chi, J. C. Kim, N. H. Hur, K. W. Lee, and Y. N. Choi, *Phys. Rev. B* **68**, 172402 (2003).

⁷D. Fruchart and E. F. Bertaut, *J. Phys. Soc. Jpn.* **44**, 781 (1978).

⁸B. S. Wang, J. C. Lin, P. Tong, L. Zhang, W. J. Lu, X. B. Zhu, Z. R. Yang, W. H. Song, J. M. Dai, and Y. P. Sun, *J. Appl. Phys.* **108**, 093925 (2010).

⁹P. Tong, Y. P. Sun, B. C. Zhao, X. B. Zhu, and W. H. Song, *Solid State Commun.* **138**, 64 (2006).

¹⁰F. Grandjean and A. Gerard, *J. Phys. F* **6**, 451 (1976).

¹¹A. Kenmotsu, T. Shinohara, and H. Watanabe, *J. Phys. Soc. Jpn.* **32**, 377 (1972).

¹²J. Y. Fan, L. S. Ling, B. Hong, L. Zhang, L. Pi, and Y. H. Zhang, *Phys. Rev. B* **81**, 144426 (2010).

¹³K. Ghosh, C. J. Lobb, R. L. Greene, S. G. Karabashev, D. A. Shulyatev, A. A. Arsenov, and Y. Mukovskii, *Phys. Rev. Lett.* **81**, 4740 (1998).

¹⁴L. Zhang, J. Y. Fan, L. Li, R. W. Li, L. S. Ling, Z. Qu, W. Tong, S. Tan, and Y. H. Zhang, *Eurphys. Lett.* **91**, 57001 (2010).

¹⁵A. K. Pramanik and A. Banerjee, *Phys. Rev. B* **79**, 214426 (2009).

¹⁶R. G. Butters and H. P. Myers, *Philos. Mag.* **46**, 895 (1955).

¹⁷N. Khan, A. Midya, K. Mydeen, P. Mandal, A. Loidl, and D. Prabhakaran, *Phys. Rev. B* **82**, 064422 (2010).

¹⁸A. Arrott, *Phys. Rev.* **108**, 1394 (1957).

¹⁹B. K. Banerjee, *Phys. Lett.* **12**, 16 (1964).

²⁰M. E. Fisher, *Rep. Prog. Phys.* **30**, 615 (1967).

²¹H. E. Stanley, *Introduction to Phase Transitions and Critical Phenomena* (Oxford University Press, London, 1971).

²²J. S. Kouvel and M. E. Fisher, *Phys. Rev. A* **136**, A1626 (1964).

²³L. P. Kadanoff, *Physics* **2**, 263 (1966).

²⁴A. Arrott and J. E. Noakes, *Phys. Rev. Lett.* **19**, 786 (1967).

²⁵A. Perumal, V. Srinivas, V. V. Rao, and R. A. Dunlap, *Phys. Rev. Lett.* **91**, 137202 (2003).

²⁶J. Mira, J. Rivas, M. Vazquez, J. M. Garcia-Beneytez, J. Arcas, R. D. Sanchez, and M. A. Senaris-Rodriguez, *Phys. Rev. B* **59**, 123 (1999).

²⁷M. E. Fisher, S. Ma, and B. G. Nickel, *Phys. Rev. Lett.* **29**, 917 (1972).

²⁸S. F. Fischer, S. N. Kaul, and H. Kronmuller, *Phys. Rev. B* **65**, 064443 (2002).

²⁹K. Motizuki and H. Nagai, *J. Phys. C* **21**, 5251 (1988).

³⁰J. H. Shim, S. K. Kwon, and B. I. Min, *Phys. Rev. B* **66**, 020406(R) (2002).

³¹K. Huang, *Statistical Mechanics*, 2nd ed. (Wiley, New York, 1987).

³²S. N. Kaul, *J. Magn. Mater.* **53**, 5 (1985).